Published in final edited form as:
Sci Signal. ; 1(35): ra1. doi:10.1126/scisignal.1159945.

The Extracellular Calcium-Sensing Receptor (CaSR) Is a Critical Modulator of Skeletal Development

Wenhan Chang[*,†], **Chialing Tu**[*], **Tsui-Hua Chen**, **Daniel Bikle**, and **Dolores Shoback**
Endocrine Research Unit, Department of Veterans Affairs Medical Center, Department of Medicine, University of California, San Francisco, CA 94121, USA

Abstract

The extracellular Ca^{2+}-sensing receptor (CaSR) plays a nonredundant role in the functions of the parathyroid gland (PTG) and the kidney. Severe hyperparathyroidism, premature death, and incomplete gene excision in *Casr*$^{-/-}$ mice have precluded the assessment of CaSR function in other tissues. We generated mice with tissue-specific deletion of *Casr* in the PTG, bone, or cartilage. Deletion of *Casr* in the PTG or bone resulted in profound bone defects, whereas deletion of *Casr* in chondrocytes (cartilage-producing cells) resulted in death before embryonic day 13 (E13). Mice in which chondrocyte-specific deletion of *Casr* was induced between E16 and E18 were viable but showed delayed growth plate development. Our data show a critical role for the CaSR in early embryogenesis and skeletal development.

Introduction

Changes in the concentration of extracellular Ca^{2+} ($[Ca^{2+}]_e$) modulate diverse biological activities, such as secretion, neurotransmission, muscle contraction, and coagulation (1–3). To maintain systemic Ca^{2+} homeostasis, land-dwelling tetrapods developed skeletons to serve as Ca^{2+} reservoirs, which, together with complex hormonal systems to transport Ca^{2+} into and out of bone, meet the body's demands for Ca^{2+}. Parathyroid cells (PTCs) are the first responders in the control of systemic Ca^{2+} homeostasis. When the $[Ca^{2+}]_e$ falls below a certain threshold, PTCs rapidly release parathyroid hormone (PTH), which increases bone resorption, releasing Ca^{2+} from the bone matrix into the circulation, and promotes renal Ca^{2+} reabsorption. Both actions tend to restore the serum $[Ca^{2+}]$ to normal. Chronically, PTH increases 1,25-dihydroxyvitamin D_3 production to enhance intestinal Ca^{2+} absorption. When the $[Ca^{2+}]_e$ increases, the release of PTH and the transcription of its gene are suppressed, and the above responses are muted.

The extracellular Ca^{2+}-sensing receptor (CaSR), a guanine triphosphate (GTP)–binding protein (G protein)–coupled receptor (GPCR), couples changes in $[Ca^{2+}]_e$ to signaling responses in PTCs (2, 3). Heterozygous and homozygous inactivating mutations in *Casr* cause familial benign hypocalciuric hypercalcemia (FBHH) and neonatal severe hyperparathyroidism (NSHPT), respectively (1, 2, 4). Patients with these disorders have mildly to severely elevated serum PTH concentrations [hyperparathyroidism (HPT)] and high serum $[Ca^{2+}]$ (hypercalcemia) depending on gene-dosage effects. Despite hypercalcemia, patients with FBHH and NSHPT have inappropriately low urinary $[Ca^{2+}]$ (hypocalciuria), confirming that renal CaSRs are required for appropriate Ca^{2+} excretion in response to hypercalcemia. Patients with NSHPT have severe skeletal demineralization at birth, which is thought to be due to severe HPT. The presence of CaSRs in bone and

[†]To whom correspondence should be addressed. wenhan.chang@ucsf.edu.
[*]These authors contributed equally to this work.

cartilage has, however, raised the question of whether defective signaling of CaSRs in bone cells, chondrocytes, or both may contribute to the skeletal phenotype in NSHPT.

Studies in vitro implicate a role for high $[Ca^{2+}]_e$ in enhancing the differentiation of osteoblasts (5, 6) and growth plate chondrocytes (GPCs) (7, 8). CaSRs are found in both cell types (9), but it has been difficult to show a role for these receptors in skeletal development in vivo. Although generalized *Casr* knockout (KO) mice ($Casr^{-/-}$) (10) exhibit severe rickets and growth retardation (11), this phenotype is rescued when the $Casr^{-/-}$ mice are bred with mice lacking parathyroid glands (PTGs) (12) or with mice with an inability to synthesize PTH (13). This finding led to the idea that HPT alone causes the skeletal abnormalities in $Casr^{-/-}$ mice and that the absence of CaSRs in bone and cartilage does not contribute to skeletal pathology (12, 13).

A critical aspect of $Casr^{-/-}$ mice that has come to light is that knockout of the receptor is incomplete because of the alternative splicing of *Casr*. In the growth plate (14), skin (15), and kidney (15) of these mice, an alternatively spliced *Casr* transcript, which lacks exon 5, is generated. The neomycin-resistance gene cassette was inserted into exon 5 to disrupt *Casr* expression in this model. RNA splicing allows for the expression of a truncated CaSR lacking 77 amino acid residues in its extracellular domain, which are encoded by exon 5 (14). Our studies (14) support the hypothesis that this spliced receptor compensates for the absence of full-length CaSRs in tissues such as bone and cartilage in $Casr^{-/-}$ mice and that this renders this knockout incomplete. Whether the compensation is partial or full has not been established. To determine definitively the role of CaSRs in skeletal development, we generated conditional knockouts of *Casr* in parathyroid, bone, and cartilage cells. Our findings support a requirement for the CaSR in bone growth and mineralization by modulating functions of PTCs, osteoblasts, and GPCs.

Results

Generation of a floxed *Casr* mouse

We first produced mice with loxP sites flanking exon 7 of *Casr*, which are referred to hereafter as floxed *Casr* mice. Exon 7 encodes the seven transmembrane domains and four intracellular loops of the CaSR. The targeting strategy used to introduce loxP sequences into 129/SvJae embryonic stem (ES) cells and the generation of floxed *Casr* mice are described in Materials and Methods (Fig. 1A). The complete integration of the loxP sites into the genome of the ES cells before blastocyst injections and the generation of the resulting floxed *Casr* mice were confirmed by polymerase chain reaction (PCR) analyses of genomic DNAs with three different sets of primers (Fig. 1B; see table S1 for primer sequences). To confirm that Cre recombinase could excise exon 7, genomic DNAs were incubated with bacteriophage P1 Cre recombinase in vitro. As confirmed by PCR analyses, the enzyme efficiently excised floxed *Casr* alleles in DNA from ES cells and from heterozygous and homozygous floxed *Casr* mice (Fig. 1C).

Although this knockout strategy enabled the transcription of exons 1 to 6, which encode the extracellular domain (amino acid residues 1 to 577) of the CaSR, this truncated protein (ΔExon7-CaSR) does not activate phospholipase C (PLC) as assessed by the inability of human embryonic kidney (HEK) 293 cells expressing ΔExon7-CaSR complementary DNA (cDNA) to produce [^{3}H]inositol phosphates (InsPs) from [^{3}H]inositol-labeled membrane polyphosphoinositides. The ΔExon7-CaSR receptor fails to increase total InsP production in response to increasing $[Ca^{2+}]_e$ to 20 mM when compared with cells expressing the full-length [also referred to as wild-type (WT)] CaSR (fig. S1). Expression of the ΔExon7-CaSR cDNA also does not interfere with the function of the full-length CaSR. When HEK 293 cells separately transfected with cDNAs encoding full-length CaSR or ΔExon7-CaSR were

subsequently mixed, cultured together, and then tested for InsP responses, there was no alteration in the sensitivity or magnitude of these responses to high $[Ca^{2+}]_e$ in cells expressing full-length CaSRs (fig. S1).

To confirm the physiological role of the CaSR in PTCs, which was demonstrated previously in *Casr*$^{-/-}$ mice (10), and to examine the contribution of HPT mediated by PTC-specific deletion of *Casr* to skeletal development in vivo, we bred floxed *Casr* mice with mice expressing Cre recombinase cDNA under the control of the *PTH* promoter (*PTH-Cre*)(16) to produce PTC-specific *Casr* KO mice. Heterozygous (^{PT}*Casr*$^{WT/\Delta flox}$, PT-Het) and homozygous KO (^{PT}Casr$^{\Delta flox/\Delta flox}$, PT-KO) mice were born in the expected Mendelian ratios. Control littermates had one or two floxed *Casr* alleles and no *PTH-Cre* transgene. Whereas PT-Het mice developed normally, the growth of PT-KO mice was severely blunted, and they died within 2 weeks of birth, with weights about 45% of those of control and PT-Het mice (Fig. 2A and Table 1). Analyses of genomic DNA confirmed that the genotypes were correct (Fig. 2B) and that excision of exon 7 (ΔExon 7) was restricted to PTGs and had not occurred in bone, cartilage, or other tissues (Fig. 2C). Western blotting showed that the abundance of full-length CaSR protein had been reduced by about 70% in PTGs from PT-Het mice and by more than 95% in PTGs from PT-KO mice compared with that in control mice (Fig. 2D). A band of about 90 kD corresponding to the ΔExon7-CaSR protein was detected in PT-Het and PT-KO PTGs, but not in the PTGs of control littermates (Fig. 2D).

Quantitative real-time PCR (qPCR) performed with primers targeted to the junction of exons 6 and 7 of *Casr* confirmed strong knockdown of *Casr* messenger RNA (mRNA) (by about 90%) in the PTGs of PT-KO mice (Fig. 2E). We observed a greater (about twofold) abundance of Casr mRNA in the PTGs of PT-Het mice compared with that in control mice, which is indicative either of an increased rate of *Casr* transcription or of the stabilization of *Casr* mRNA in response to hypercalcemia or another biochemical abnormality in these mice. This is further supported by the increased abundance of ΔExon7-CaSR mRNA in the PT-KO mice, as detected by qPCR with primers specific for the junction of exons 2 and 3 of *Casr* (Fig. 2E). Despite the increased abundance of mRNA, the abundance of ΔExon7-CaSR protein in PTGs of PT-KO mice was about 10% of that of full-length CaSR protein in the PTGs of control mice (Fig. 2D), which suggests that the truncated protein has a reduced half-life compared with that of the full-length protein.

The abundance of PTH mRNA in PTGs from PT-Het and PT-KO mice was significantly increased compared with that of control mice (Fig. 2E), compatible with the elevated concentrations of serum PTH and serum Ca^{2+} observed in vivo (Table 1). There was a clear effect of gene dosage as evidenced by the occurrence of mild HPT in PT-Het mice and severe HPT in the PT-KO mice (Table 1). In contrast to the hypocalciuria of *Casr*$^{-/-}$ mice (10), PT-Het and PT-KO mice had urinary $[Ca^{2+}]$ about 25% and 380% higher than that of control mice, respectively (Table 1). As expected, intact renal CaSRs promoted Ca^{2+} excretion in the normal physiologic response to hypercalcemia.

Knockout of *Casr* in PTCs retards skeletal development

Whole-mount alizarin red (AR) and Alcian blue (AB) staining of 2-week-old mice showed that PT-KO mice had multiple rib and tibial fractures and smaller and severely undermineralized skeletons compared with those of control and PT-Het littermates (Fig. 3A). To further confirm the reduced mineral content of their skeletons, we performed micro-computed tomography (μCT) on the femurs of PT-KO mice to quantify precisely the amount of mineral present by measuring the density of hydroxyapatite, the dominant form of bone mineral. Three-dimensional (3D) reconstructed images from the μCT scans revealed poorly mineralized matrix and the lack of secondary ossification centers in the epiphyses

(tracing in red) compared with the femurs of control mice (Fig. 3B). Histological analyses of bone sections after von Kossa (VK) staining (to detect phosphate-containing minerals) and safranin O (SO) counterstaining (to detect proteoglycan) showed substantially reduced mineral deposition in trabecular (Tb) and cortical (Ct) bones in PT-KO mice compared with those in control mice (Fig. 3C). Goldner trichrome staining of adjacent sections revealed excessive undermineralized osteoid (pink) mixed with mineralized matrix (green) in PT-KO mice (Fig. 3C), which was suggestive of defective bone formation.

To determine whether these defects were due to delayed osteoblast differentiation, function, or both, we examined the expression of genes encoding osteoblast-specific markers and regulators of differentiation. The expression of both early and late osteogenic genes, including *osterix*(*OSX*), *type I collagen*[*Col(I)*], *alkaline phosphatase*(*ALP*), *dentin matrix protein 1*(*DMP1*), *osteocalcin*(*OCN*), and *sclerostin*(*SOST*), was profoundly decreased in the bones of 14-day-old PT-KO mice compared with those of control mice (Fig. 3D), indicating a delay in osteoblast differentiation. We found that the expression of *Casr* mRNA was more than 70% lower in the bones of PT-KO mice than in those of control mice (Fig. 3D), despite our inability to document any excision of *Casr* in bone (Fig. 2C). These data suggest that the severe HPT and hypercalcemia that were due to PTC-specific knockout of *Casr* affected early skeletal development. This likely occurred because of increased PTH receptor signaling that was accompanied by reduced *Casr* expression in the bones of the PT-KO mice.

The bones of PT-Het mice were indistinguishable from those of control mice at 2 weeks of age, as assessed by whole-mount staining, μCT scans, and qPCR analyses. The abundance of *Casr* mRNA in the bones of PT-Het mice was equivalent to that of control mice. Mild osteopenia (reduced bone mineral density) was, however, evident in PT-Het mice by 6 months of age, as demonstrated by μCT of Tb bone in the distal femur and of Ct bone at the tibia–fibula junction (TFJ) (Fig. 3, E and F). The trabecular bone volume (BV), an index of the amount of bone mineral present in a given tissue volume (TV), was significantly decreased when expressed as the ratio of Tb.BV to TV (Fig. 3F). Tb thickness (Th) and Tb numbers (N) were also reduced. These findings could be due to decreased bone formation by osteoblasts, increased bone resorption by osteoclasts, or a combination of the two. Tb connectivity density (CD) and Tb spacing (Sp), which reflect the state of the Tb microarchitecture, in the PT-Het mice were not significantly different from those of control mice (Fig. 3F). In the other bone compartment, namely, Ct bone, Ct. TV Ct.BV and Ct.Th were also significantly decreased in PT-Het mice compared with those of control mice (Fig. 3F), indicating that the smaller bones of the PT-Het animals had thinner cortices. Thus, long-term albeit mild HPT has cumulative, age-dependent effects on skeletal homeostasis.

Impaired postnatal growth and skeletal development in mice with osteoblasts deficient in *Casr*

To determine the role of the CaSR in osteoblasts, we generated osteoblast-specific *Casr* KO mice by breeding floxed *Casr* mice with mice expressing the *Cre* transgene driven by the 2.3-kb *Col(I)* α_1 subunit promoter [2.3Col(I)-*Cre*], which is expressed in the early- and late-stage cells of the osteoblast lineage (17). Genomic analyses by PCR confirmed the excision of exon 7 of *Casr* in bones from either heterozygous ($^{\text{Col-Bone}}Casr^{\text{WT/}\Delta\text{flox}}$, COL-Het) or homozygous KO ($^{\text{Col-Bone}}Casr^{\Delta\text{flox/}\Delta\text{flox}}$, COL-KO) mice, but not from those of control littermates (fig. S2).

COL-Het mice grew and developed similarly to their control littermates. Deletion of both alleles of the *Casr* gene in osteoblasts, however, profoundly blocked postnatal growth and skeletal development in the COL-KO mice. This was evident by 3 days of age, and by day 20, the body weights of COL-KO mice were about 30% of those of control and COL-Het

littermates (Fig. 4A). Whole-mount AR and AB staining showed that the COL-KO mice had smaller and severely undermineralized skeletons compared with those of control mice, which was visible by 5 days (Fig. 4B). The skeletons and body weights of COL-Het mice were comparable with those of control littermates through the first 3 weeks of age (Fig. 4, A and B). Most COL-KO mice had rib and long bone fractures and died within 3 weeks of birth. Undermineralization of the skull (Fig. 4C, arrowheads), vertebrae (double arrows), and long bones (arrows) of COL-KO mice was confirmed by μCT analyses. The latter studies showed markedly decreased Tb.BV, Tb.BV/TV, Tb.Th, and Tb.N in the distal femurs of COL-KO mice compared with those of control mice, which suggests the impaired ability of osteoblasts to form bone in the skeletons of COL-KO mice. This was supported by the finding of a decreased Tb.CD and increased Tb.Sp, hallmarks of osteopenia and aweakened Tb architecture or structure, in the COL-KO mice. In addition, the reduction in cortical parameters (Ct.TV, Ct. BV, and Ct.Th) at the TFJ in COL-KO mice compared with control mice (Fig. 4D) indicated that the impact of *Casr* knockout was general and evident at different skeletal sites and different types of bone. Consistent with the μCT data was the histological staining for mineralization, which showed that bones from COL-KO mice contained large quantities of undermineralized osteoid (pink by Goldner staining), which was mixed with normally mineralized matrix (green by Goldner, black by VK staining) (Fig. 4E).

Consistent with poor mineralization, as assessed by histological analyses, qPCR showed the markedly decreased expression of genes encoding both early and late markers of osteoblast differentiation, such as *Col(I)*, *ALP*, *DMP1*, *OCN*, and *SOST*, in bones from 7-day-old COL-KO mice compared with those of control mice (Fig. 4F). However, *OSX* expression in the COL-KO mice was comparable with that of control mice, indicating that the changes due to deletion of *Casr* occurred after the expression of *OSX*. Similar changes in gene expression as well as bone histology were also evident in newborn mice (<1 day old) (fig. S3), which suggests that skeletal defects developed prenatally. In addition to changes in the abundance of markers of differentiation, *Casr* knockout in osteoblasts significantly suppressed the expression of the gene encoding insulin-like growth factor 1 (IGF-1) (Fig. 4F), a growth factor critical for osteoblast survival and differentiation, suggesting that the CaSR may modulate osteoblast differentiation by altering the local abundance of IGF-1. Although cyclin D1 (*CCND1*) expression was significantly increased in COL-KO mice compared with that in control mice, the expression of the genes encoding the prosurvival factors B cell lymphoma/leukemia 2 (Bcl-2) and Bcl-2– like 1 (Bcl-2L1) (18, 19) was profoundly suppressed. We also found increased expression of *interleukin-10* (*IL-10*), an inducer of apoptosis in other cells (20), in COL-KO compared with that in control mice (Fig. 4F). These observations suggested the increased occurrence of apoptosis, which was confirmed by the detection of enhanced terminal deoxynucleotidyl transferase–mediated deoxyuridine triphosphate nick end labeling (TUNEL) staining in apoptotic osteoblasts and osteocytes in sections from COL-KO mice compared with those from control mice (Fig. 4G).

Because the expression of *Col(I)* is low in tissues such as liver, skin, testis, ovary, and kidney (17), we considered the possibility that the early death of the COL-KO mice might be due to reduced *Casr* expression in other tissues. To address this, we used a different targeting strategy to generate osteoblast-specific *Casr* KO mice. We bred floxed *Casr* mice with mice expressing the *Cre* transgene controlled by an *OSX* promoter [*OSX-Cre*](21). *OSX* expression is restricted to osteoblasts and their precursors and occurs before the expression of *Col(I)* but after that of *Runx2* (21). The OSX-Cre construct induces Cre-lox recombination in osteoblasts during embryonic development and early postnatal life (21).

Genomic DNA analyses showed that excision of exon 7 of *Casr* in heterozygous ($^{\text{Osx-Bone}}Casr^{\text{WT/}\Delta\text{flox}}$, OSX-Het) and homozygous KO ($^{\text{Osx-Bone}}Casr^{\Delta\text{flox/}\Delta\text{flox}}$, OSX-KO)

mice occurred only in bone and not in other tissues (Fig. 5A) and did not occur in bone from control mice. As was seen in COL-KO mice, knockout of both *Casr* alleles in OSX-KO osteoblasts profoundly blocked postnatal growth and skeletal development (Fig. 5, B to D). Reduced bone formation and mineralization, confirmed by the alterations in μCT parameters, were evident in both Tb and Ct bones in 4-week-old OSX-KO mice. They showed decreased Tb.BV, Tb.BV/TV, Tb.Th, Tb.N, and Tb.CD and increased Tb.Sp in the distal femur and decreases in Ct.TV and Ct.BV at the TFJ (Fig. 5, C and D). Phenotypic abnormalities were also evident in newborn mice (<1 day old) with decreased expression of the genes encoding the osteoblast markers *Col(I)* and *OCN* in bones from newborn OSX-KO mice by qPCR (Fig. 5E). Taken together, these data support a role for the CaSR in modulating the growth and differentiation of osteoblasts, a paradigm essential for orderly postnatal skeletal development.

Delayed growth plate development and embryonic death following GPC-specific deletion of *Casr*

Studies with mouse GPCs support roles for high $[Ca^{2+}]_e$ and the CaSR in promoting differentiation (8, 14). To determine the role of CaSR in the growth plate in vivo, we targeted chondrocytes by breeding floxed *Casr* mice with mice expressing the *Cre* transgene under the control of the type *II collagen α1subunit*[*Col(II)*] (Cart) promoter [*Col(II)-Cre*] (22). No homozygous knockout ($^{Cart}Casr^{\Delta flox/\Delta flox}$, Cart-KO) mice were born alive from 35 litters (~350 pups). In addition, no Cart-KO mouse embryos were detectable at E14 to E16 from 8 litters or at later time points. In 56 embryos from 6 litters at the E12 to E13 stage, only two Cart-KO embryos of confirmed genotype were found, indicating that most of these embryos died earlier (fig. S4). Skeletons from the two surviving E12.5 Cart-KO embryos were shorter than those of control and heterozygous ($^{Cart}CaSR^{WT/\Delta flox}$, Cart-Het) littermates and had poorly mineralized rib cages, calvariae, and long bones (as demonstrated by lack of AR staining) (Fig. 6A). These data suggest that blocking *Casr* expression in *Col(II)*-expressing cells severely impedes viability beyond E12 to E13 and inhibits early steps in cartilage and bone mineralization.

Because knockout of *Casr* in *CoI(II)*-expressing cells is lethal, we developed a tamoxifen (Tam)-inducible knockout model [$^{Tam\text{-}Cart}Casr^{\Delta flox/\Delta flox}$, Tam-Cart-KO] to examine the role of CaSR at later stages of embryonic and postnatal development of GPCs. We used transgenic ($^{Cart}Cre\text{-}ER^{Tam}$) mice that express a fusion protein (Cre-ER^{Tam}) of the Cre recombinase fused to a mutated ligand-binding domain of the estrogen receptor (ER^{Tam}) under the control of a mouse *Col(II)* promoter (23). In this model, trans-location of the Cre-ER^{Tam} protein to the nucleus, an essential step for Cre-lox recombination, only occurs when Tam, or its derivative 4OH-Tam, is administered to the mice (23). The ability of Tam to specifically induce *Cre* activity in cartilage has been confirmed previously (23, 24). We bred the $^{Cart}Cre\text{-}ER^{Tam}$ mice with $Casr^{flox/flox}$ mice to obtain $^{Cart}Cre\text{-}ER^{Tam(+/-)}Casr^{flox/flox}$ mice, which were viable and fertile in the absence of Tam. We next crossed the ^{Cart}Cre-$ER^{Tam(+/-)}Casr^{flox/flox}$ mice with $Casr^{flox/flox}$ mice to obtain experimental animals: ^{Cart}Cre-$ER^{Tam(+/-)}Casr^{flox/flox}$ (~50%) and $Casr^{flox/flox}$ (~50%) mice. Both sets of mice were treated with either 4OH-Tam or vehicle, which resulted in the generation of three strains of mice: induced homozygous *Casr* KO mice ($^{Tam\text{-}Cart}Casr^{\Delta flox/\Delta flox}$, Tam-Cart-KO) and the controls, $Casr^{flox/flox}$ mice exposed to 4OH-Tam and ^{Cart}Cre-$ER^{Tam(+/-)}Casr^{flox/flox}$ mice exposed to vehicle (Fig. 6B).

To delete *Casr* before birth, pregnant mice were injected with a single dose of 4OH-Tam (1.5 mg) or vehicle at E16 to E17, and the embryos were analyzed 48 to 72 hours after injection. The genotypes of $^{Cart}Cre\text{-}ER^{Tam(+/-)}Casr^{flox/flox}$ and $Casr^{flox/flox}$ mice and the ability of 4OH-Tam to induce excision of exon 7 in the former mice were confirmed by genomic DNA analyses (Fig. 6B). Whole-mount AR and AB staining showed a ~10%

reduction in the overall length of the skeletons of 4OH-Tam–treated Tam-Cart KO mice compared with those of treated *Casr*$^{flox/flox}$ control mice, which included shorter humeri, femurs, and tibiae (Fig. 6C). Immunohistochemical analyses confirmed a marked reduction in the abundance of the CaSR in the hypertrophic zones of tibial growth plates of 4OH-Tam–treated Tam-Cart-KO mice compared with that of treated control mice (Fig. 6D), which was indicative of prompt (within 48–72 hours) knockdown of *Casr* expression.

Further evidence of *Casr* knockdown was provided by qPCR analysis, which showed the decreased expression of full-length *Casr* mRNA in growth plates from 4OH-Tam–treated Tam-Cart-KO growth plates (Fig. 6F). In cartilage sections stained by VK and SO reagents, there was ~20% expansion of the hypertrophic zone and decreased mineral deposition in that zone in 4OH-Tam–treated Tam-Cart-KO mice compared with that in treated control mice (Fig. 6E). qPCR analyses of epiphyseal growth plates showed decreased expression of *type X collagen* [*Col(X)*], *RUNX2*, and *osteopontin* (*OPN*), which are markers of mature and terminally differentiated chondrocytes, in Tam-Cart-KO compared with control mice (Fig. 6F). The expression of genes encoding early differentiation markers, such as *aggrecan* (*AGG*) and *Col(II)*, was unchanged (Fig. 6F), supporting a selective delay in chondrocyte maturation and terminal differentiation in Tam-Cart-KO mice.

Insulin-like growth factor 1 signaling is a critical pathway that promotes chondrocyte differentiation (25). We examined whether this pathway was affected by the knockout of *Casr* in the GPCs of Tam-Cart-KO mice. Immunohistochemical and qPCR analyses showed significant reductions in the expression of *IGF-1* and *IGF-1 receptor* (*IGF-1R*) mRNAs (Fig. 6F) and in the abundance of their protein products (Fig. 7A) in the growth plate of Tam-Cart-KO mice compared with those of control mice. To test whether reduced IGF-1R signaling affected the differentiation of GPCs, we performed in vitro knockout of *IGF-1R* by infecting GPCs from floxed *IGF-1R* mice with adenoviruses expressing Cre recombinase (Ad-Cre) or empty vector (Ad-Cont). Knockdown of *IGF-1R* mRNA and loss of IGF-1R protein in the Ad-Cre–infected GPCs were confirmed by qPCR (Fig. 7B) and Western blotting (Fig. 7C), respectively. These changes were accompanied by a significant reduction in the expression of *Col(X)* mRNA (Fig. 7B) and in mineral deposition (Fig. 7D) in the Ad-Cre–infected cells compared with that in Ad-Cont–infected cells. These data support the concept that knockdown of *Casr* delays GPC differentiation in Tam-Cart-KO mice, at least in part by the reduction of IGF-1R signaling in these cells.

Discussion

CaSRs are broadly present in bone, brain, gut, skin, and endocrine glands, and changes in $[Ca^{2+}]_e$ alter cell function in these tissues. Whether the CaSR is the mediator of all aspects of Ca^{2+}-sensing in these tissues in vivo has not been easy to address because of the lack of suitable animal models. The floxed *Casr* mouse strain that we have developed is the first model that permits tissue-specific deletion of *Casr*.

We showed that Cre recombinase excised floxed *Casr* alleles in three tissues critical to Ca^{2+} homeostasis and skeletal development. The PTC-specific *Casr* KO mouse provided proof of concept for the gene-targeting strategy we used, because these mice showed severe HPT and hypercalcemia, despite having normal renal responsiveness to Ca^{2+}. Heterozygous and homozygous PTC-specific *Casr* KO mice showed the expected mild and severe HPT, respectively, with a clear gene dosage effect, similar to the phenotype of generalized *Casr*$^{-/-}$ mice (10). We noted that the degree of HPT in PTC-specific *Casr* KO mice appeared to be more severe than that of the generalized KO model (10), with serum PTH concentrations in PT-Het and PT-KO mice that were ~2- to 3- and 17-fold higher, respectively, than those of control littermates (Table 1). In contrast, the abundance of serum PTH in generalized

Casr$^{+/-}$ and *Casr*$^{-/-}$ mice was only ~0.5- and 9.5-fold higher, respectively, than that of control mice (10). This raises the possibility that the alternatively spliced *Casr* mRNA, which lacks exon 5, might also be expressed in PTCs in the generalized *Casr*$^{-/-}$ mouse (10) and so mediate some degree of Ca^{2+}-sensing (10). To confirm this will require direct comparison of the responsiveness of PTCs to Ca^{2+} in these two mouse models, which will be challenging. Alternatively, different breeding conditions, diets, mouse strains, and PTH assays may explain the differences in the biochemical phenotypes.

Data from experiments performed in PT-KO mice confirmed that severe HPT impeded bone growth and mineralization, as was seen in generalized *Casr*$^{-/-}$ mice (10). We further show that this is accompanied by the reduced expression of genes encoding markers of osteoblast differentiation. This recapitulates the effects of continuous PTH treatment on both the differentiation of osteoblasts and the formation of mineralized nodules in culture (26, 27). In contrast, the milder HPT observed in PT-Het mice produced osteopenia later in life, which is similar to the classic presentation of primary HPT in humans. The molecular basis for the effects of HPT on skeletal development remains to be elucidated. PTH mediates signaling through the receptor activator of nuclear factor κB lig-and (RANK-L)/RANK/ osteoprotegerin (28, 29) and Wnt (30) pathways, obvious candidate pathways to interrogate in the future.

We unexpectedly observed a marked reduction in the abundance of the CaSR in the bones of PT-KO mice, which suggests that loss of CaSR signaling in that tissue may also contribute to skeletal pathology. This idea is supported by the presence of skeletal defects in both models of *Casr* KO in osteoblasts (COL-KO and OSX-KO). As well as blocking differentiation, deletion of *Casr* in the bones of COL-KO mice reduced the expression of *IGF*-1 and increased the expression of *IL-10* compared with that in control mice. Because IGF-1 signaling in osteoblasts is critical for cell survival and because *IL-10* is proapoptotic, changes in the abundance of these factors in bone would be expected to promote cell death, particularly in cells of the osteoblast lineage. This was confirmed by the presence of increased TUNEL staining in osteoblasts and osteocytes from COL-KO mice compared with that in control mice. Taken together, these data suggest that CaSR signaling modulates the proliferation, survival, and differentiation of osteoblasts, potentially by altering growth and survival factors elaborated by bone.

The embryonic lethality of the chondrocyte-specific *Casr* KO mouse was unexpected. Generalized *Casr*$^{-/-}$ mice (10), which were developed by a different targeting strategy, live for several days postnatally and survive for a longer period if HPT is prevented (12, 13). This has been interpreted as evidence that the CaSR is not critical for embryonic development. In light of data from the Cart-KO mouse, we suspect that alternatively spliced *Casr* mRNAs, which lack exon 5, are present in the generalized *Casr*$^{-/-}$ mice and can compensate for as yet undefined functions of CaSRs in the embryo. The delayed cartilage maturation and mineralization observed in the two E12.5 Cart-KO embryos we studied support a role for the CaSR in the early stages of growth plate formation. It has been reported that Col(II) is transiently expressed in heart valves in mice between E10.5 and E14.5 (31). Thus, knockdown of *Casr* at that site might affect cardiac development and function and lead to embryonic death, but this remains to be determined.

Because Cart-KO embryos were nonviable, we turned to an inducible KO model. Tam-induced KO of the expression of *Casr* in GPCs produced a rickets-like phenotype with expansion and reduced mineralization of the hypertrophic zone and the decreased abundance of markers of mature, terminally differentiated chondrocytes within 2 to 3 days of exposure to Tam. These observations are consistent with work by us and others that show that high $[Ca^{2+}]_e$ promotes chondrocyte differentiation and that suppressing *Casr* expression with

antisense or dominant-negative cDNA constructs blocks this effect (9, 32, 33). Furthermore, our data indicate that reduced local IGF-1R signaling plays at least some part in delaying GPC differentiation in the KO mice. Taken together, these data are the first to definitively establish a role for the CaSR in Ca^{2+} sensing in GPCs.

In summary, this study provides the first evidence supporting the direct involvement of CaSR signaling in the differentiation of osteoblasts and GPCs and skeletal development in vivo and suggests that inhibition of *Casr* expression in bone in states of HPT maybe part of the mechanism underlying the skeletal defects in this disorder. These floxed *Casr* mice will enable future definitive assessment of CaSR function in other tissues.

Materials and Methods

Construction of the gene-targeting vector and production of floxed *Casr* mice

The targeting construct contained three loxP sites flanking exon 7 of *Casr* and the cytidine deaminase (CD)–neomycin (NEO) gene cassette (Fig. 1A). The targeting construct was transfected into 129/SvJae ES cells to allow homologous recombination with endogenous *Casr* alleles, and cells were selected with G418 and fialuridine. The resulting floxed *Casr* ES cells were injected into C57/BL6 blastocysts and implanted into pseudo-pregnant CD1 mice to produce chimeric mice (University of California San Francisco Transgenic Core Facility). Chimeras were bred with C57/BL6 mice to produce heterozygous floxed *Casr* (*Casr*$^{wt/flox}$) mice through germline transmission. *Casr*$^{wt/flox}$ mice were interbred to produce homozygous floxed *Casr* (*Casr*$^{flox/flox}$) mice. Integration of the targeting construct into the genome of floxed *Casr* ES cells before blastocyst injections and the genotypes of the resulting *Casr*$^{wt/flox}$ and *Casr*$^{flox/flox}$ mice were confirmed by PCR with three sets of primers targeting different regions of the construct (Fig. 1A; see table S1 for primer sequences), P1U/P1L, P2U/P2L, and P3U/P3L, which amplified cDNAs with sizes of ~1800, 1050, and 167 bp, respectively, from the floxed *Casr* allele. All mice were maintained under standard conditions with free access to food and water under protocols approved by the Animal Care Subcommittee, San Francisco Department of Veterans Affairs Medical Center.

Generation and genotyping of conditional *Casr* knockout mice

Mice with KO of *Casr* specifically in PTCs, osteoblasts, or chondrocytes were generated by breeding *Casr*$^{flox/flox}$ mice with transgenic mice expressing *Cre*-recombinase under the control of the appropriate promoter: the *PTH* promoter (*PTH-Cre*, The Jackson Laboratory) for PTCs, the 2.3-kb fragment of the rat *Col(I)* promoter [2.3*Col(I)-Cre*; gift of Dr. Barbara Kream, University of Connecticut, Farmington] or the *OSX* promoter [*OSX-Cre*, gift of Dr. Andrew McMahon, Harvard University (21)] for osteoblasts, and the mouse *Col(II)* promoter [*Col(II)-Cre*, The Jackson Laboratory] for chondrocytes. To generate Tam-inducible *Casr* knockout in cartilage, we bred the floxed *Casr* mice with transgenic mice [^{Cart}Cre-ER^{Tam}; a gift of Dr. Susan Mackem, National Institutes of Health (NIH)] expressing a fusion protein (Cre-ER^{Tam}) of Cre recombinase and a mutated ligand-binding domain of the estrogen receptor (ER^{Tam}) under the control of a mouse *Col(II)* promoter and enhancer. The inducibility of Cre activity by Tam and the specific expression of the construct in cartilage has been previously confirmed (23, 24). Mouse genotypes were determined by PCR analyses of genomic DNAs from tail snips with primers for the *Cre* transgene (Cre-1/Cre-2; see table S2), which amplified a ~500-bp cDNA and the P3U and P3L primer set for the loxP sequence at the 3′ end of exon 7, which amplified a 133-bp DNA fragment from wild-type alleles and a 167-bp DNA from floxed *Casr* alleles. To verify tissue-specific gene excision, genomic DNA was isolated from the tissues specified and was then subjected to PCR analysis with the P4/P3L primer set, which amplified a 284-bp DNA fragment from the *Casr* gene allele after the excision of exon 7.

Whole-mount AR and AB staining

Mice were skinned, eviscerated, and fixed in ethanol (95%) for 2 to 5 days. Tissues were then defatted in acetone for 2 days, stained in AR/AB solution [AB (0.015%), AR (0.005%), acetic acid (0.05%), and ethanol (75%)] for 5 days, cleared in KOH (1%) in glycerol (gradually increased from 0% to 20%, 50%, and 80% with 2-day intervals between steps), and stored and visualized in 100% glycerol (34).

Von Kossa and Goldner staining

Femurs and tibiae were isolated, fixed in 10% phosphate-buffered formalin, dehydrated, defatted, and embedded in plastic (methyl methacrylate, Sigma, St. Louis, MO). For detection of phosphate-containing minerals, 4-μm sections were stained with VK reagents by a standard protocol (35) [silver nitrate (1%) in H_2O for 10 min in the dark; a mixture of sodium carbonate (5%) and formaldehyde (10%) in H_2O for 2 min; and a mixture of sodium thiosulfate (10%) and potassium ferricyanide (0.05%) in H_2O for 20 s; with washes in tap water between steps], followed by counterstaining with SO (0.01%) in H_2O for 20 min. To distinguish between mineralized matrix and unmineralized osteoid, sections were stained with Goldner trichrome reagents [in H_2O, picric acid (1%) at 37°C for 2 hours; fuchsin (1%) for 15 min; phosphomolybdic acid (6%) for 5 min; and light green (4%) for 15 min; with washes in tap water between steps].

Cell culture, transfection, and [^{3}H]InsP assay

HEK 293 cells were cultured and transfected with WT-CaSR-green fluorescent protein (GFP), ΔExon7-CaSR-GFP, WT-CaSR, ΔExon7-CaSR, or empty pcDNA3.1 vector cDNAs (10 μg/construct) as described (36). Twenty-four hours after transfection, cells were replated on coverslips for confocal microscopy, six-well dishes for [^{3}H]InsP assays, and 10-cm dishes for protein lysates and cultured for an additional 48 hours. For coculture experiments, cells separately transfected with WT-CaSR or with ΔExon7-CaSR cDNAs were mixed in a 1:1 ratio and cocultured for 48 hours before the start of InsP assays. Twenty-four hours after re-plating, HEK 293 cells expressing WT-CaSR or ΔExon7-CaSR cDNAs and a mixture of cells expressing each of these constructs were labeled with [^{3}H]myoinositol (2 μCi/ml) for 18 to 24 hours (36). Cells were exposed to conditions of differing $[Ca^{2+}]_e$ for 60 min at 37°C after pre-treatment for 10 min with 10 mM LiCl. Total [^{3}H]InsP was quantified after anion-exchange chromatography and is presented as the fold increase over the basal amount of [^{3}H]InsP under conditions of 0.5 mM Ca^{2+} and 0.5 mM Mg^{2+}.

Immunocytochemistry and Western blotting

For fluorescent microscopy, HEK 293 cells transfected with WT-CaSR-GFP or ΔExon7-CaSR-GFP and grown on coverslips were fixed with 4% paraformaldehyde, mounted on glass slides with Gel Mount (Biomeda, Foster City, CA), and examined with a Leica TCS confocal microscope (Laboratory for Cell Imaging, San Francisco Department of Veterans Affairs Medical Center). Tibiae from E18 to E19 Tam-Cart-KO and control embryos were dissected, fixed in 4% paraformaldehyde in phosphate-buffered saline (PBS), decalcified in 10% EDTA in PBS for 24 hours, and cut into 4-μm sections. Immunoreactivity in these sections was detected with a custom-made rabbit polyclonal anti-CaSR antibody (100 nM) raised against an intracellular epitope of the receptor (36) and horseradish peroxidase (HRP)–conjugated goat antirabbit immunoglobulin G antisera, and signals were developed by a 3,3′-diaminobenzidine (DAB) substrate. Sections were counterstained with aqueous hematoxylin. Proteins from total cell lysates of HEK 293 cells expressing WT-CaSR-GFP or ΔExon7-CaSR-GFP and from concentrated culture media bathing the cells were electrophoresed on SDS–polyacrylamide gel electrophoresis gels and transferred to nitrocellulose membranes (36). Membranes were incubated with anti-GFP (50 nM) antibody

and the appropriate HRP-conjugated secondary antibodies. Signals were detected with a SuperSignal chemiluminescence substrate and developed on Kodak x-ray film.

Microcomputed tomography

To quantify the amount of mineral deposited by mature osteoblasts in the bone matrix, we performed μCT scans at two anatomical sites: the distal femur, a site rich in Tb bone, and the TFJ, a site rich in Ct bone, as described (35). Femurs and tibiae were isolated, fixed in 10% phosphate-buffered formalin for 24 hours, and then switched to 70% ethanol. Bones were then scanned in a tube containing 70% ethanol by a Scanco vivaCT 40 scanner (Scanco Medical, Basserdorf, Switzerland). To assess Tb bone in the distal femoral metaphysis, 100 serial cross-sectional scans (1.05 mm) of the secondary spongiosa were obtained from the end of the growth plate, extending proximally with 10.5-μm voxel size and 55-kV x-ray energy. For the Ct bone scans, 100 serial cross sections (1.05 mm) of the tibia were obtained from the TFJ, extending proximally with 10.5-μm voxel size and 55-kV x-ray energy. For analysis of μCT images, thresholds were applied to segment or separate the mineralized bone matrix from soft tissue. Linear attenuation was calibrated with hydroxyapatite as the standard. Image analysis and 3D reconstructions were performed with the manufacturer's software (SCANCO Medical AG, Bassersdorf, Switzerland).

Quantitative real-time PCR assays

RNA samples isolated from the PTGs of 2-week-old mice, from the humeral cortices of 14- and 21-day-old mice after the bone marrow was flushed out, or from epiphyseal growth plates from E18 to E19 embryos were reverse-transcribed into cDNA and subjected to qPCR (7, 8). Expression of the following genes was determined: *Casr* and *PTH* for PTGs; osteogenic markers [*OSX*, *Col(I)*, *ALP*, *DMP1*, *OCN*, *SOST*] and *Casr* and the growth regulatory factors *IGF-1*, *CCND1*, *Bcl-2*, *Bcl-2L1*, and *IL-10* for bone; and chondrogenic markers [*AGG*, *Col(II)*, *Col(X)*, *OPN*, and *RUNX2*] and *IGF-1*, *IGF-1R*, and *Casr* for cartilage. Taqman assay– based sets of primers and probes for mouse *Casr* (spanning exons 6 and 7), *PTH*, *CCND1*, *DMP1*, and *SOST* were obtained from Applied Biosystems (Foster City, CA). Cyber green–based sets of primers and probes for *Bcl-2*, *Bcl-2L1*, *IL-10*, and *GAPDH* were purchased from SuperArray (Frederick, MD). Taqman-based sets of primers and probes for *OSX*, *Col(I)*, *ALP*, *OCN*, *Casr* (spanning exons 2 and 3), *AGG*, *Col(II)*, *Col(X)*, *IGF-1*, *IGF-1R*, *RUNX2*, *OPN*, and *L19* were custom-made by Integrated DNA Technologies (Coralville, IA) according to published sequences (table S2).

Culture, adenoviral infection, and AR staining of floxed *IGF-1R* GPCs

Growth plate chondrocytes isolated from 2- to 4-day-old floxed *IGF-1R* mice (37) were cultured and infected with replication-deficient adenoviruses [~16 plaque-forming units (PFU)/cell] carrying cDNA encoding the bacterial Cre recombinase (Ad-Cre) or no insert (Ad-Cont) as described (38). RNA and cell lysates were isolated 48 to 72 hours post-infection to assess the expression of *IGF-1R* and $\alpha_1(X)$ as described above. Alizarin red staining was performed on infected cultures grown in medium containing 2.0 mM Ca^{2+} for 14 days to assess mineralization (8).

Statistics

Data from two groups were represented as mean ± the standard error of the mean and compared by unpaired Student's *t* test. Significance was assigned for $P < 0.05$ or $P < 0.01$.

Supplementary Material

Refer to Web version on PubMed Central for supplementary material.

Acknowledgments

We acknowledge B. Kream (University of Connecticut, Farmington), A. McMahon (Harvard University), and S. Mackem (NIH, Bethesda, MD) for providing 2.3Col(I)-Cre, OSX-Cre, and CartCre-ERTam mice, respectively, and R. Nissenson (Endocrine Unit, University of California, San Francisco) for helpful discussions in the planning and completion of these studies. This work was supported by NIH RO1-AG21353 (W.C.), R21-AR50662 (W.C.), RO1-AR050023 (D.B.), and P01-AR39448 (D.B.), by the Department of Veteran Affairs Merit Review (D.S. and D.B.) and Research Education Advancement Program in Bone Disease (W.C., D.B., and D.S.), and by the Department of Defense-U.S. Army Medical Research and Materiel Command W81XWH-05-2-0094 (W.C. and D.S).

References and Notes

1. Brown EM. The calcium-sensing receptor: Physiology, pathophysiology and CaR-based therapeutics. Subcell Biochem. 2007; 45:139–167. [PubMed: 18193637]
2. Brown EM, MacLeod RJ. Extracellular calcium sensing and extracellular calcium signaling. Physiol Rev. 2001; 81:239–297. [PubMed: 11152759]
3. Chang W, Shoback D. Extracellular Ca^{2+}-sensing receptors—an overview. Cell Calcium. 2004; 35:183–196. [PubMed: 15200142]
4. Brown, EM.; Bai, M.; Pollak, M. Familial benign hypocalciuric hypercalcemia and other syndromes of altered responsiveness to extracellular calcium. In: Avioli, LV.; Krane, SM., editors. Metabolic Bone Disease. Academic Press; New York: 1998. p. 479-499.
5. Dvorak MM, Siddiqua A, Ward DT, Carter DH, Dallas SL, Nemeth EF, Riccardi D. Physiological changes in extracellular calcium concentration directly control osteoblast function in the absence of calciotropic hormones. Proc Natl Acad Sci USA. 2004; 101:5140–5145. [PubMed: 15051872]
6. Dvorak MM, Riccardi D. Ca^{2+} as an extracellular signal in bone. Cell Calcium. 2004; 35:249–255. [PubMed: 15200148]
7. Chang W, Rodriguez L, Chen TH, Tu C, Shoback D. Extracellular Ca^{2+}-sensing in cartilage. J Musculoskelet Neuronal Interact. 2004; 4:410–411. [PubMed: 15758285]
8. Rodriguez L, Cheng Z, Chen TH, Tu C, Chang W. Extracellular calcium and parathyroid hormone–related peptide signaling modulate the pace of growth plate chondrocyte differentiation. Endocrinology. 2005; 146:4597–4608. [PubMed: 16099862]
9. Chang W, Tu C, Chen TH, Komuves L, Oda Y, Pratt SA, Miller S, Shoback D. Expression and signal transduction of calcium-sensing receptors in cartilage and bone. Endocrinology. 1999; 140:5883–5893. [PubMed: 10579354]
10. Ho C, Conner DA, Pollak MR, Ladd DJ, Kifor O, Warren HB, Brown EM, Seidman JG, Seidman CE. A mouse model of human familial hypocalciuric hypercalcemia and neonatal severe hyperparathyroidism. Nat Genet. 1995; 11:389–394. see comments. [PubMed: 7493018]
11. Garner SC, Pi M, Tu Q, Quarles LD. Rickets in cation-sensing receptor-deficient mice: An unexpected skeletal phenotype. Endocrinology. 2001; 142:3996–4005. [PubMed: 11517179]
12. Tu Q, Pi M, Karsenty G, Simpson L, Liu S, Quarles LD. Rescue of the skeletal phenotype in CasR-deficient mice by transfer onto the Gcm2 null background. J Clin Invest. 2003; 111:1029–1037. [PubMed: 12671052]
13. Kos CH, Karaplis AC, Peng JB, Hediger MA, Goltzman D, Mohammad KS, Guise TA, Pollak MR. The calcium-sensing receptor is required for normal calcium homeostasis independent of parathyroid hormone. J Clin Invest. 2003; 111:1021–1028. [PubMed: 12671051]
14. Rodriguez L, Tu C, Cheng Z, Chen TH, Bikle D, Shoback D, Chang W. Expression and functional assessment of an alternatively spliced extracellular Ca^{2+}-sensing receptor in growth plate chondrocytes. Endocrinology. 2005; 146:5294–5303. [PubMed: 16166224]
15. Oda Y, Tu CL, Chang W, Crumrine D, Komuves L, Mauro T, Elias PM, Bikle DD. The calcium sensing receptor and its alternatively spliced form in murine epidermal differentiation. J Biol Chem. 2000; 275:1183–1190. [PubMed: 10625662]
16. Libutti SK, Crabtree JS, Lorang D, Burns AL, Mazzanti C, Hewitt SM, O'Connor S, Ward JM, Emmert-Buck MR, Remaley A, Miller M, Turner E, Alexander HR, Arnold A, Marx SJ, Collins FS, Spiegel AM. Parathyroid gland-specific deletion of the mouse Men1 gene results in

parathyroid neoplasia and hypercalcemic hyperparathyroidism. Cancer Res. 2003; 63:8022–8028. [PubMed: 14633735]

17. Liu F, Woitge HW, Braut A, Kronenberg MS, Lichtler AC, Mina M, Kream BE. Expression and activity of osteoblast-targeted Cre recombinase transgenes in murine skeletal tissues. Int J Dev Biol. 2004; 48:645–653. [PubMed: 15470637]
18. McGill GG, Horstmann M, Widlund HR, Du J, Motyckova G, Nishimura EK, Lin YL, Ramaswamy S, Avery W, Ding HF, Jordan SA, Jackson IJ, Korsmeyer SJ, Golub TR, Fisher DE. Bcl2 regulation by the melanocyte master regulator Mitf modulates lineage survival and melanoma cell viability. Cell. 2002; 109:707–718. [PubMed: 12086670]
19. Wiren KM, Toombs AR, Semirale AA, Zhang X. Osteoblast and osteocyte apoptosis associated with androgen action in bone: Requirement of increased Bax/Bcl-2 ratio. Bone. 2006; 38:637–651. [PubMed: 16413235]
20. Pestka S, Krause CD, Sarkar D, Walter MR, Shi Y, Fisher PB. Interleukin-10 and related cytokines and receptors. Annu Rev Immunol. 2004; 22:929–979. [PubMed: 15032600]
21. Rodda SJ, McMahon AP. Distinct roles for Hedgehog and canonical Wnt signaling in specification, differentiation and maintenance of osteoblast progenitors. Development. 2006; 133:3231–3244. [PubMed: 16854976]
22. Ovchinnikov DA, Deng JM, Ogunrinu G, Behringer RR. Col2a1-directed expression of Cre recombinase in differentiating chondrocytes in transgenic mice. Genesis. 2000; 26:145–146. [PubMed: 10686612]
23. Nakamura E, Nguyen MT, Mackem S. Kinetics of tamoxifen-regulated Cre activity in mice using a cartilage-specific CreER(T) to assay temporal activity windows along the proximodistal limb skeleton. Dev Dyn. 2006; 235:2603–2612. [PubMed: 16894608]
24. Maeda Y, Nakamura E, Nguyen MT, Suva LJ, Swain FL, Razzaque MS, Mackem S, Lanske B. Indian Hedgehog produced by postnatal chondrocytes is essential for maintaining a growth plate and trabecular bone. Proc Natl Acad Sci USA. 2007; 104:6382–6387. [PubMed: 17409191]
25. Wang Y, Nishida S, Sakata T, Elalieh HZ, Chang W, Halloran BP, Doty SB, Bikle DD. Insulin-like growth factor-I is essential for embryonic bone development. Endocrinology. 2006; 147:4753–4761. [PubMed: 16857753]
26. Bellows CG, Ishida H, Aubin JE, Heersche JN. Parathyroid hormone reversibly suppresses the differentiation of osteoprogenitor cells into functional osteoblasts. Endocrinology. 1990; 127:3111–3116. [PubMed: 2174346]
27. Ishizuya T, Yokose S, Hori M, Noda T, Suda T, Yoshiki S, Yamaguchi A. Parathyroid hormone exerts disparate effects on osteoblast differentiation depending on exposure time in rat osteoblastic cells. J Clin Invest. 1997; 99:2961–2970. [PubMed: 9185520]
28. Liao J, McCauley LK. Skeletal metastasis: Established and emerging roles of parathyroid hormone related protein (PTHrP). Cancer Metastasis Rev. 2006; 25:559–571. [PubMed: 17165129]
29. Huang JC, Sakata T, Pfleger LL, Bencsik M, Halloran BP, Bikle DD, Nissenson RA. PTH differentially regulates expression of RANKL and OPG. J Bone Miner Res. 2004; 19:235–244. [PubMed: 14969393]
30. Bergenstock MK, Partridge NC. Parathyroid hormone stimulation of noncanonical Wnt signaling in bone. Ann N Y Acad Sci. 2007; 1116:354–359. [PubMed: 18083937]
31. Rahkonen O, Savontaus M, Abdelwahid E, Vuorio E, Jokinen E. Expression patterns of cartilage collagens and Sox9 during mouse heart development. Histochem Cell Biol. 2003; 120:103–110. [PubMed: 12883905]
32. Chang W, Tu C, Pratt S, Chen TH, Shoback D. Extracellular Ca(2+)-sensing receptors modulate matrix production and mineralization in chondrogenic RCJ3.1C5.18 cells. Endocrinology. 2002; 143:1467–1474. [PubMed: 11897705]
33. Chang W, Tu C, Bajra R, Komuves L, Miller S, Strewler G, Shoback D. Calcium sensing in cultured chondrogenic RCJ3.1C5.18 cells. Endocrinology. 1999; 140:1911–1919. [PubMed: 10098531]
34. McLeod MJ. Differential staining of cartilage and bone in whole mouse fetuses by Alcian blue and alizarin red S. Teratology. 1980; 22:299–301. [PubMed: 6165088]

35. Dvorak MM, Chen TH, Orwoll B, Garvey C, Chang W, Bikle DD, Shoback DM. Constitutive activity of the osteoblast Ca^{2+}-sensing receptor promotes loss of cancellous bone. Endocrinology. 2007; 148:3156–3163. [PubMed: 17412806]

36. Chang W, Pratt S, Chen TH, Nemeth E, Huang Z, Shoback D. Coupling of calcium receptors to inositol phosphate and cyclic AMP generation in mammalian cells and Xenopus laevis oocytes and immunodetection of receptor protein by region-specific antipeptide antisera. J Bone Miner Res. 1998; 13:570–580. [PubMed: 9556057]

37. Zhang M, Xuan S, Bouxsein ML, von Stechow D, Akeno N, Faugere MC, Malluche H, Zhao G, Rosen CJ, Efstratiadis A, Clemens TL. Osteoblast-specific knockout of the insulin-like growth factor (IGF) receptor gene reveals an essential role of IGF signaling in bone matrix mineralization. J Biol Chem. 2002; 277:44005–44012. [PubMed: 12215457]

38. Cheng Z, Tu C, Rodriguez L, Chen TH, Dvorak MM, Margeta M, Gassmann M, Bettler B, Shoback D, Chang W. Type B gamma-aminobutyric acid receptors modulate the function of the extracellular Ca^{2+}-sensing receptor and cell differentiation in murine growth plate chondrocytes. Endocrinology. 2007; 148:4984–4992. [PubMed: 17615148]

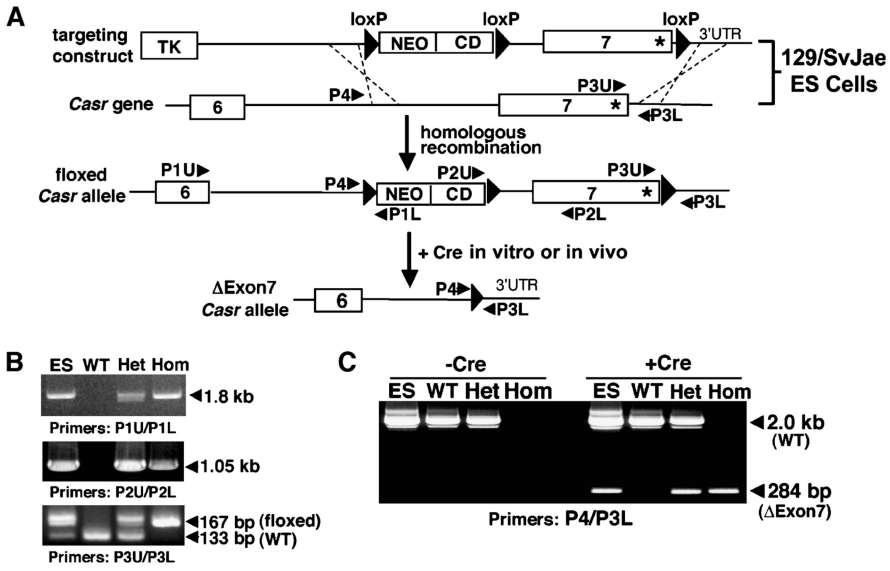

Fig. 1.

Generation of floxed *Casr* mice. (**A**) The gene-targeting strategy used to introduce loxP sequences to flank exon 7 of *Casr* required a construct containing three loxP sites flanking exon 7 of the *Casr* gene and the cytidine deaminase (CD)–neomycin (NEO) gene cassette. This construct was trans-fected into 129/SvJae ES cells to allow homologous recombination with endogenous *Casr* alleles. The resulting floxed *Casr*-containing ES cells were injected into C57/BL6 blastocysts to produce chimeric mice that were bred to obtain heterozygous ($Casr^{wt/flox}$) and homozygous ($Casr^{flox/flox}$) mice. (**B**) PCR analyses of genomic DNAs from floxed *Casr*-containing ES cells before blastocyst injection and from the tails of $Casr^{wt/wt}$ (WT), heterozygous $Casr^{wt/flox}$ (Het), and homozygous $Casr^{flox/flox}$ (Hom) mice were performed with specific primers (see Materials and Methods) to confirm integration of the targeting sequences. (**C**) PCR analyses of genomic DNAs from (**B**) after incubation with (+Cre) or without (−Cre) bacteriophage P1 Cre recombinase in vitro for 30 min. The 284-bp band represents the DNA fragment due to excision of exon 7 (ΔExon7).

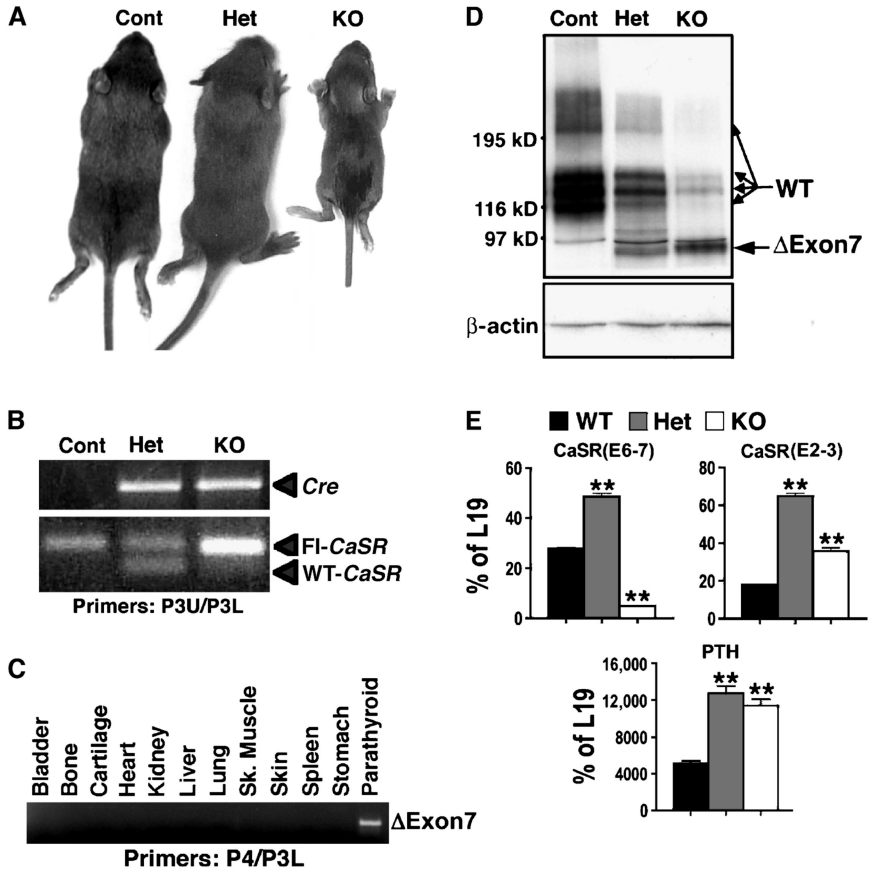

Fig. 2.

Heterozygous and homozygous deletion of the *Casr* gene in parathyroid cells (PTCs) produces mild and severe hyperparathyroidism (HPT), respectively. (**A**) Two-week-old PT-KO ($^{PT}CaSR^{\Delta flox/\Delta flox}$) mice showed severe growth retardation, with body weights about 45% of that of their control and PT-Het ($^{PT}CaSR^{WT/\Delta flox}$) littermates. (**B**) PCR analyses of genomic DNAs confirmed the expression of the *Cre* trans-gene and floxed *Casr* alleles in PT-Het and PT-KO mice. The control mice used in this experiment were $CaSR^{flox/flox}$, which do not express *Cre*. (**C**) PCR analyses of genomic DNAs from tissues of PT-KO mice confirmed the deletion of exon 7 only in PTGs. (D) Western blotting of PTG lysates showed the decreased abundance of full-length CaSR protein (WT, 120 to 250 kD) by ~70% and >95% in the PT-Het and PT-KO mice, respectively, compared with control littermates. PTG ly-sates from PT-Het and PT-KO mice contained the ΔExon7-CaSR (ΔExon7) protein (about 90 kD), which was encoded by exons 1 to 6. (**E**) qPCR analyses with primers flanking the junctions of either exons 6 and 7 (E6-7) or exons 2 and 3 (E2-3) of *Casr* and primers specific for PTH mRNA were presented as the percentage of expression of the gene encoding the mitochondrial ribosomal protein L19 (** $P < 0.01$, $n = 4$ to 6 mice).

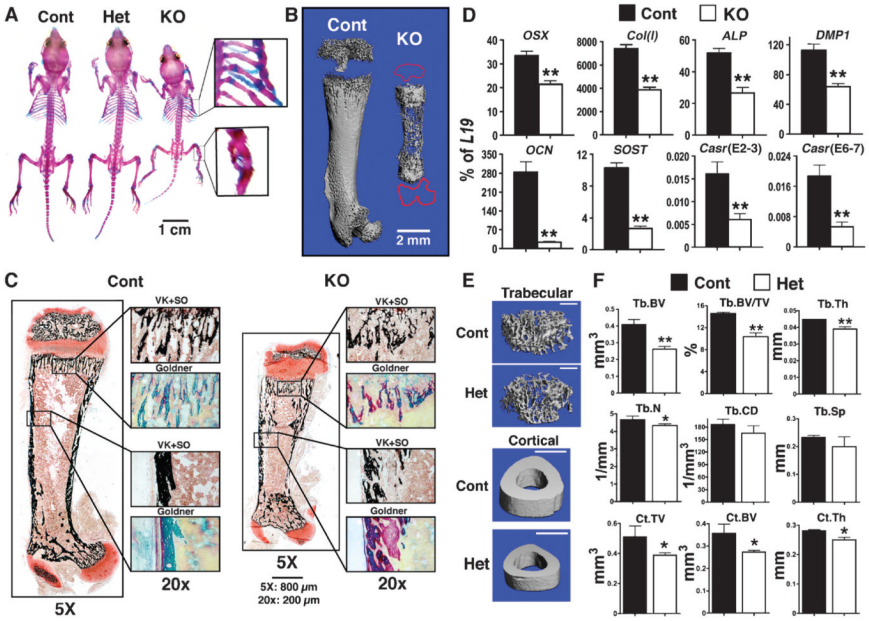

Fig. 3.

Knockout of *Casr* in PTCs impedes skeletal development. (**A**) Whole-mount AR and AB staining showed a smaller skeleton with fractures in the ribs and tibiae (see insets) of 14-day-old PT-KO ($^{PT}Casr^{\Delta flox/\Delta flox}$) mice, but not in PT-Het ($^{PT}CaSR^{WT/\Delta flox}$) orcontrol mice. (**B**) Reconstructed 3D μCT images of femurs from 14-day-old PT-KO mice showed severely undermineralized matrix compared with those of control mice. (**C**) Histological analyses of femurs from PT-KO mice showed reduced mineralization and osteoid accumulation. Consecutive plastic-embedded femur sections from 14-day-old control and PT-KO mice stained with VK reagents and counterstained with SO or Goldner reagents were visualized at 5× magnification. Boxes in the right panels are enlarged regions of interest (reproduced at 20×). Scale bars: 800 μm at 5×; 200 μm at 20×. (**D**) Gene expression studies indicated the delayed differentiation of osteoblasts in bones from PT-KO mice compared with that of control mice. qPCR analyses of genes encoding osteoblast markers were performed on RNA isolated from humeral cortices (no marrow) of 14-day-old mice. All measurements of gene expression are presented as the percentage of *L19* expression (**P* < 0.05, ***P* < 0.01; *n* = 6 to 8 mice). Expression of *OSX*, *Col(I)*, *ALP*, *DMP1*, *OCN*, and *SOST* in PT-KO mice was reduced by 36%, 48%, 48%, 43%, 91%, and 74%, respectively, compared with that in control mice. PCR analyses with primers flanking the junctions of exons 6 and 7 (E6-7) or exons 2 and 3 (E2-3) of *Casr* showed reductions in both transcripts in bone in which the *PTH-Cre* transgene was not expressed. (**E**) Reconstructed 3D μCT images of Tb bone in distal femurs and Ct bone at the TFJ of 6-month-old control and PT-Het mice. Scale bars: 1 mm for all panels. (**F**) μCT parameters assessed were BV, BV/TV, Th, N, CD, and Sp for Tb bone and TV, BV, and Th for Ct bone (defined in Results; **P* < 0.05, ***P* < 0.01; *n* = 6 to 8 mice).

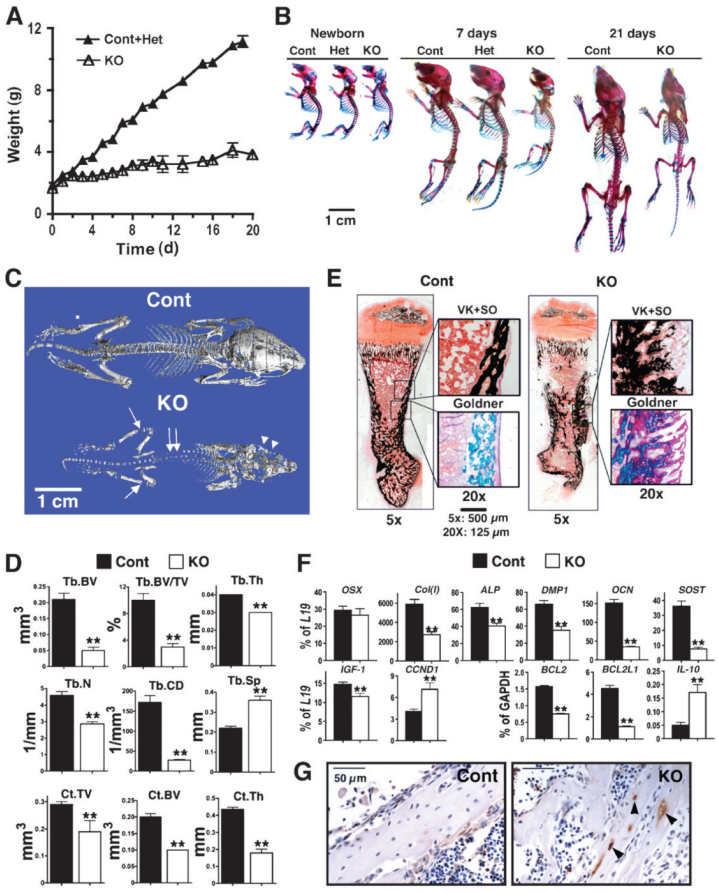

Fig. 4.

Knockout of *Casr* in osteoblasts, driven by 2.*3Col(I)-Cre*, blocked growth and skeletal development. (**A**) Body weights of control (n = 8), heterozygous ($^{\text{Col-}Bone}Casr^{\text{WT/}\Delta\text{flox}}$, COL-Het, $n = 12$), and homozygous KO ($^{\text{Col-}Bone}Casr^{\Delta\text{flox/}\Delta\text{flox}}$, COL-KO, $n = 9$) mice from birth until postnatal day 20. Because the weights of control and Het mice were indistinguishable, they were combined and are presented as Cont+Het. COL-KO mice exhibited growth retardation, which was evident by postnatal day 3. (**B**) Whole-mount AR and AB staining showed that the skeletons of COL-KO mice were smaller than those of control and heterozygous mice at postnatal day 5. (**C**) Reconstructed 3D μCT images of skeletons from 20-day-old mice showed severe undermineralization in COL-KO mice, evident in the skull (arrowheads), vertebrae (double arrows), and long bones (arrows). (**D**) μCT parameters of Tb bone in the distal femur (Tb.BV, Tb.BV/TV, Tb.Th, Tb.N, Tb.CD, and Tb.Sp) and Ct bone at the TFJ (Ct.TV, Ct.BV, and Ct.Th) of 20-day-old control and COL-KO mice showed statistically significant reductions in all parameters except Tb. Sp, which was markedly increased—all of which were confirmatory of reduced bone mass and microarchitecture (**$P < 0.01$; $n = 6$ mice). (**E**) Histological analyses of femurs from COL-KO mice showed poor mineralization and osteoid accumulation compared with those of control mice. VK+SO and Goldner staining were performed on consecutive plastic-embedded sections from 7-day-old control and COL-KO femurs and visualized at 5× magnification. Boxes in the right panels are enlarged regions of interest (reproduced at 20×). Scale bars: 500 μm (5×); 125 μm (20×). (**F**) The expression of genes encoding osteoblast markers indicated delayed differentiation in COL-KO mice compared with that in control mice. qPCR analyses of samples isolated from humeral cortices (no marrow) from 14-day-old mice with primers specific for *OSX*, *Col(I)*, *ALP*, *DMP1*, *OCN*, *SOST*, *IGF*-1, *CCND1*,

Bcl-2, *Bcl-2L1*, and *IL-10* were performed. Results are presented as the percentage of expression of *L19* or *glyceraldehyde 3-phosphate dehydrogenase* (*GAPDH*) (** $P < 0.01$; $n =$ 6 to 9 mice). Reductions (percent decrease in COL-KO mice compared with control mice) of 54%, 35%, 47%, 77%, 79%, and 22% were seen in the expression of *Col(I)*, *ALP*, *DMP1*, *OCN*, *SOST*, and *IGF*-1, respectively. (**G**) TUNEL staining of femoral cortex from 7-day-old control and KO mice with hematoxylin counter-staining. TUNEL-positive cells are indicated by brown DAB stain (arrowheads) ($n = 8$ sections from four mice).

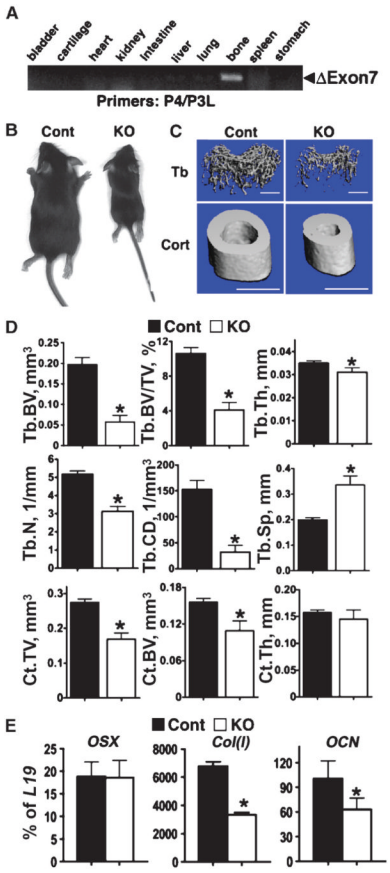

Fig. 5.

Knockout of floxed *Casr* in osteoblasts by *OSX-Cre* results in retarded growth and altered gene expression. (**A**) PCR analyses of genomic DNAs confirmed that deletion of exon 7 occurred only in bone from homozygous $^{\text{Osx-Bone}}Casr^{\Delta\text{flox}/\Delta\text{flox}}$ (OSX-KO) mice and not in other tissues. (**B**) One-month-old OSX-KO mice were growth-retarded compared with control mice. (**C**) μCT images of trabecular (Tb) and cortical (Ct) bones in the distal femur and TFJ, respectively, showed severely under-mineralized matrix in 4-week-old KO mice compared with that in control mice. Scale bars: 1 mm for all panels. (**D**) μCT parameters assessed included BV, BV/TV, Th,N,CD, and SpforTbbone and TV, BV, and Th for Ct bone in 4-week-old control and OSX-KO mice. (*$P < 0.01$; $n = 6$ for KO and $n = 12$ for control mice). (**E**) Analysis of gene expression by qPCR in samples isolated from humeral cortices (no marrow) of newborn mice indicated delayed differentiation of osteoblasts in OSX-KO mice compared with that of control mice, with 55% reduced expression of *Col(I)* and 35% reduced expression of *OCN*. Results are presented as the percentage of *L19* expression (*$P < 0.05$, $n = 4$ to 6 mice).

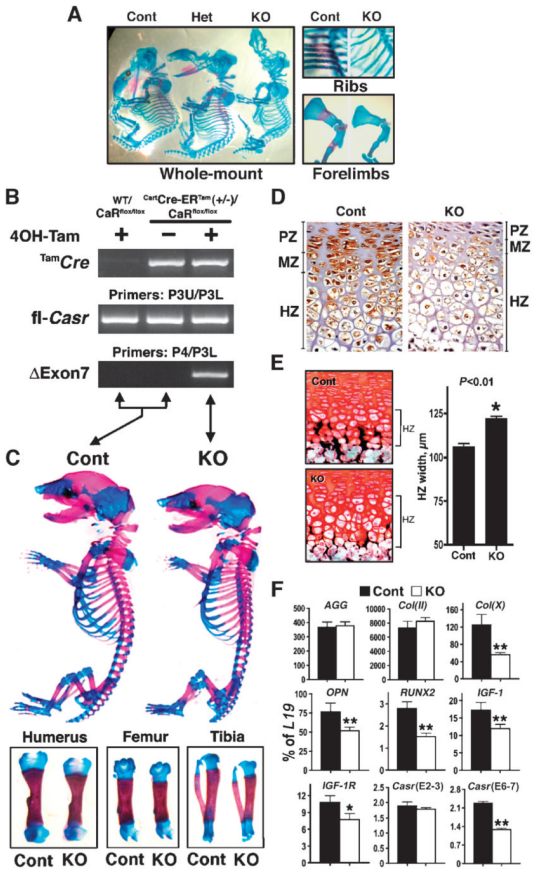

Fig. 6.

Knockout of *Casr* in chondrocytes blocks embryonic development and cartilage maturation. (**A**) Whole-mount AR and AB staining shows that the skeletons of Cart-KO ($^{Cart}Casr^{\Delta flox/\Delta flox}$) mice are smaller and undermineralized compared with those of their heterozygous ($^{Cart}Casr^{WT/\Delta flox}$) and control littermates at E12.5. (**B** to **F**) Tamoxifen (Tam)-induced knockdown of the *Casr* in cartilage produces small, undermineralized skeletons in E18-19 $^{Tam\text{-}Cart}Casr^{\Delta flox/\Delta flox}$ (Tam-Cart-KO) embryos. (**B**) PCR analysis of genomic DNAs from embryos with (+) or without (−) exposure to 4OH-Tam for the expression ofthe ^{Tam}Cre transgene, homozygous floxed Casr (fl-*Casr*) alleles, and sequences lacking exon 7 (ΔExon7). (**C**) Whole-mount AR and AB staining of E19 embryos showed smaller skeletons, including humeri, femurs, and tibiae in Tam-Cart-KO compared with those of control mice. (**D**) Immunohistochemical staining of CaSR, depicted by brown DAB staining, in the proximal tibial growth plates from E18 to E19 Tam-Cart-KO and control mice. PZ, proliferation zone; MZ, maturation zone; HZ, hypertrophic zone. (**E**) VK and SO staining of plastic sections of proximal tibial growth plates from E18 to E19 Tam-Cart-KO and control mice. The histogram presents HZ widths in proximal tibial growth plates from control and Tam-Cart-KO mice (*$P < 0.01$; $n = 4$ mice). (**F**) Gene profiling in the epiphyseal growth plates indicates a delay in cell maturation and differentiation in Tam-Cart-KO mice compared with that in control mice. qPCR was performed on epiphyseal growth plate samples from E18 to E19 Tam-Cart-KO and control mice with primers specific for early [*AGG* and *Col(II)*] and late [*Col(X)*, *OPN*, and *RUNX2*] chondrocyte markers and for *IGF-1*, *IGF-1R*, and *Casr*. Results are presented as the percentage of *L19* expression (*$P < 0.05$, **$P < 0.01$; $n = 6$ mice).

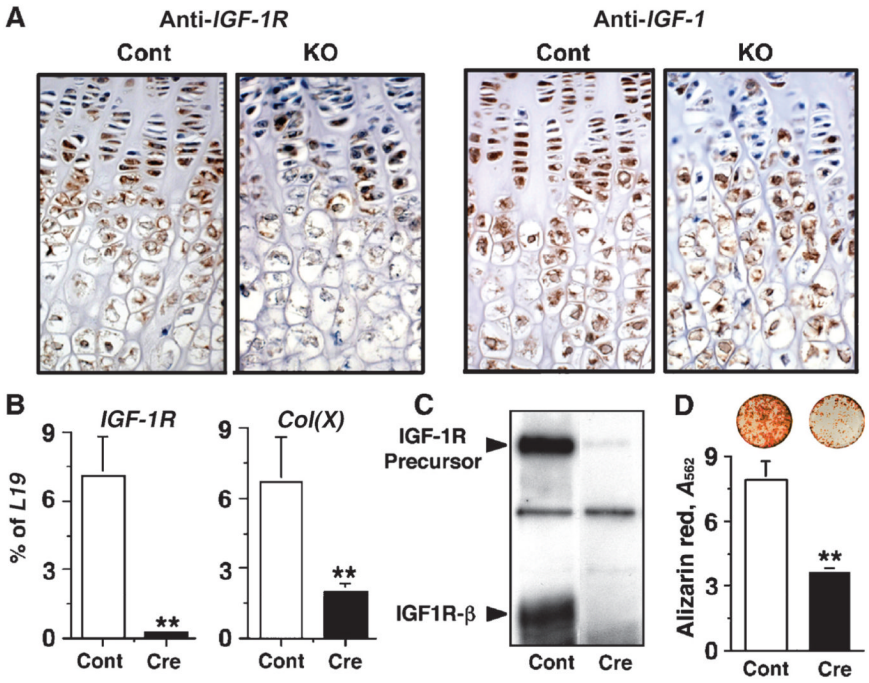

Fig. 7.

Knockout of *Casr* in chondrocytes blocks the expression of *IGF-1* and *IGF-1R* and delays cell differentiation. (**A**) Immunohistochemical staining of IGF-1 and IGF-1R, depicted by brown DAB staining, in the proximal tibial growth plates from E18 to E19 Tam-Cart-KO and control mice. (**B**) In vitro knockout of *IGF-1R* was performed by infecting floxed IGF-1R-containing GPCs with Ad-Cre (Cre) or, as a control, Ad-Cont (Cont) viruses (16 PFU/cell). Expression of *IGF-1R* and *Col(X)* mRNAs was assessed by qPCR 72 hours postinfection. (**C**) Western blots were incubated with antisera against the β subunit of IGF-1R to confirm the knockdown of IGF-1R in GPCs infected with Ad-Cre (Cre) compared with that in Ad-Cont (Cont) viruses. (**D**) AR staining was performed and quantified by absorbance to assess mineralization in cultures infected with Ad-Cre (Cre) or Ad-Cont (Cont) viruses and grown in media containing 2.0 mM Ca^{2+} for 14 days (** $P < 0.001$; $n = 3$).

Table 1

Concentrations of serum PTH, serum Ca^{2+}, and urinary Ca^{2+} and weights of PT-KO (KO), PT-Het (Het), and control (Cont) littermates.

	Cont (*n* = 19 mice)	Het (*n* = 13 mice)	KO (*n* = 11 mice)
Serum [PTH] (pg/ml)	52.7 ± 1.6	170 ± 27.4 *	959 ± 122 *
Fold over control		+2.3	+17.2
Serum [Ca^{2+}] (mg/dl)	11.6 ± 0.1	13.4 ± 0.2 *	16.4 ± 0.5 *
% Change over control		+16	+40
Urine [Ca^{2+}] (mg/dl)	2.8 ± 0.4	3.5 ± 0.5 *	13.4 ± 2.9 *
% Change over control		+25	+380
Body weight (g)	8.7 ± 0.3	8.4 ± 0.5	3.8 ± 0.4 *
% Change vs. control			−56

* $P < 0.01$.